

# Chapter 2

## Theory

In this chapter we examine Standard Model cross-section<sup>1</sup> predictions for the production of charm in hadronic collisions. The inclusive reaction can be written as follows:

$$H_B + H_T \rightarrow c\bar{c} + x' \rightarrow H_c + H_{\bar{c}} + X, \quad (2.1)$$

where  $H_B$  ( $H_T$ ) is the beam (target<sup>2</sup>) hadron,  $H_c$  ( $H_{\bar{c}}$ ) is any hadron containing a  $c$  ( $\bar{c}$ ) valence (anti)quark, and  $X$  ( $x'$ ) indicates all non-charm hadrons (partons) in the final (intermediate) state. Unitarity of the hadronization process (depicted by the arrow on the right) requires that it occur with 100% probability;<sup>3</sup> more interesting is the hard scattering (left arrow) of  $H_B$  and  $H_T$ 's constituent partons, resulting in  $c\bar{c}$  pair production. Not depicted are the weak and electromagnetic processes by which the charm and other unstable hadrons decay into stable particles.

---

<sup>1</sup>See Sections 8.1 and 9.1 for the relevant definitions.

<sup>2</sup>Although the E769 target is comprised of various nuclei, the target hadron is considered a nucleon. Support for the independence of charm production on the nuclear environment is given in Section 8.1.

<sup>3</sup>The hadronization process as written above neglects the contribution of charmonium states to the total charm particle cross-section. At the center-of-mass energy achieved by E769, however, this contribution is negligible.

## 2.1 Motivation

Calculation of a scattering amplitude, even in the context of non-relativistic time-independent quantum mechanics, is a problem often made tractable only through the use of perturbative methods, i.e., expression of the amplitude as a power-series expansion in some small parameter (say,  $g$ ). Results obtained via this procedure are necessarily approximate; their reliability (at any given order in  $g$ ) is contingent upon whether and/or how rapidly the series converges. For this reason, an important consideration is the “smallness” of  $g$ , which must be sufficient to render insignificant (at some desired level of accuracy) the error associated with truncation of the series. In practice, if the magnitude of the  $(n + 1)$ th-order term in the series cannot be well-estimated, it will be difficult to determine whether  $g$  is small enough to make an  $n$ th-order calculation useful.

For a relatively simple case, such as scattering of a non-relativistic electron by a static charge distribution, iterative procedures (e.g., the Born approximation) can be used to obtain a solution to Schrodinger’s equation expressible in powers of  $V_{int}$ , the scattering potential. In treating a more complicated case, however, for example inelastic scattering in which the destruction and creation of particles are involved, we make use of the more sophisticated formalism underlying the Standard Model of particle interactions, namely quantum field theory. In this picture, each fundamental interaction is described as acting via the exchange or “mediation” of a particular (set of) vector boson(s). Feynman, in an approach directly motivated by his “many-paths” formulation of quantum mechanics, developed a prescription for grouping and calculating all paths<sup>4</sup> contributing to a particular physical process to a given order in the coupling strength  $g$  of the theory. Each topologically distinct path, integrated over all internal momenta, can be represented by a Feynman diagram, a simple schematic

---

<sup>4</sup>In this context, “path” indicates a particular evolution in spacetime (generally entailing particle creation, destruction, and exchange) connecting sets of specified initial and final particle states. These paths must be consistent with the conservation laws obeyed by the particular interaction(s) involved and are most usefully evaluated in momentum space, with definite 4-momenta (and possibly other quantum numbers) assigned to the initial, final, and intermediate states.

in which the number of vertices indicates the relevant order in perturbation theory.<sup>5</sup> For a particular process, Feynman diagrams are readily written down and connected to the corresponding integrals via a set of Feynman rules; the amplitude for the process is then given by the sum of all contributing diagrams.

A measurable quantity such as a cross-section is proportional not to an amplitude, which is in general a complex number, but rather to the product of an amplitude and its complex conjugate (i.e., the *square* of the amplitude’s norm). Therefore, economy of expression dictates that the resulting perturbative expansion be expressed as a series in a parameter proportional to  $g^2$ , which is designated  $\alpha$ . For example, the fine-structure constant  $\alpha$  ( $\sim \frac{1}{137}$ ) of electrodynamics is equal (in CGS units) to  $\frac{e^2}{4\pi}$ , where the elementary charge  $e$  plays the role of the coupling strength  $g$ . We hereafter use the term “coupling strength” to indicate  $\alpha$  rather than  $g$ , unless otherwise specified.

In this chapter, we concern ourselves with the hadronic production of charm, a phenomenon caused by strong interactions. Although in principle this physics is sensitive at some level to electroweak effects, the extreme relative weakness of all other interactions with respect to the strong<sup>6</sup> allows us to neglect consideration of these corrections in the following discussion. The Feynman rules needed to generate the relevant diagrams are therefore all derivable from a Lagrangian containing two classes of terms: (1) kinetic terms governing the propagation of free quarks and (2) terms associated with the SU(3) color symmetry underlying Quantum Chromodynamics (QCD). These latter include terms corresponding to quark-gluon coupling, gluon-gluon coupling, and gluon kinetic energy.

“Canonical” perturbative QCD predictions for charm production are provided by Nason, Dawson, and Ellis (NDE), who have published full next-to-leading order (NLO) calculations (i.e., to order  $\alpha_S^3$ ) of total and differential cross-sections for the hadronic production of heavy quarks [36, 37]. The theorists Mangano, Nason, Ridolfi, and Frixione (in various permutations) have provided follow-up studies of these results

---

<sup>5</sup>For purposes of this discussion, we assume that all vertices in the contributing diagrams correspond to a single coupling strength  $g$ .

<sup>6</sup>Relative interaction strength depends on the distance scale at which the comparison is made, as will be discussed further in this chapter. At scales relevant to charm production, the strong coupling  $\alpha_S$  is more than fifty times greater than the electromagnetic coupling  $\alpha$ .

as well [32, 26, 38]. In the following sections, we discuss issues surrounding these calculations, followed by the numerical predictions themselves.

## 2.2 Renormalization

Evaluation of Feynman integrals is complicated by the presence of divergences, which can be classified into two types: ultraviolet and infrared. The former (latter) are associated with integrations over internal loop momenta  $k^\mu$  which diverge as  $k^\mu \rightarrow \infty$  (0).<sup>7</sup> Such infinities are a typical feature of quantum field theories, including QCD. The procedure known as renormalization, by which ultraviolet divergences are subtracted order-by-order in perturbation theory, rendering predictions finite, is well known. Without delving too deeply into technical details, we discuss some features of renormalization which are relevant to the interpretation of QCD predictions for charm hadroproduction.

Essentially, if a theory is renormalizable, each divergent diagram can be associated in a consistent manner with one or more of the input parameters of the theory (e.g., particle mass, field normalization, coupling strength) in such a way that these “bare” parameters absorb the infinities and yield analogous “renormalized” quantities which are finite. Removal of these infinities alone, however, does not completely determine these quantities; there remains some freedom in deciding what *finite* contributions of the divergent graphs will be absorbed into the definitions of the renormalized parameters. Specific prescriptions for eliminating this residual arbitrariness are called renormalization schemes and consist of fixing the values of renormalized parameters at particular mass scales. The coupling strength  $\alpha$  is defined in terms of a sum of corrected vertex diagrams evaluated at a mass scale  $\mu_R$ , which we call the renormalization scale.

An expression for a physical quantity, written as an expansion in  $\alpha$  so defined, therefore includes terms which depend on  $\mu_R$ , typically logarithmically. The scale at which we choose to “define the theory”, however, is arbitrary; this expression,

---

<sup>7</sup>If light quarks are treated as massless, infrared divergences also include infinities resulting from collinear emission by a quark or a gluon; these are called collinear or mass divergences.

evaluated at a particular order in perturbation theory, must be *independent* of  $\mu_R$ . This requirement<sup>8</sup> allows us to make the scale dependence of  $\alpha$  explicit. The resulting “running” coupling constant  $\alpha(\mu)$ , evaluated at  $\mu_R$ , can then be associated directly with each corrected vertex in a given diagram.

The expression for the dimensionless coupling  $\alpha(\mu)$  must include another mass scale; for this purpose, the fundamental scale  $\Lambda_{QCD}$  is introduced. Although the precise definition of  $\Lambda_{QCD}$  depends on the particular renormalization scheme chosen, it corresponds to the mass scale at which the coupling  $\alpha$  blows up<sup>9</sup> (more on this phenomenon later), as can be seen by the following leading-order expression:

$$\alpha_S(\mu) = \frac{1}{b_0 \ln(\mu/\Lambda_{QCD})}, \quad (2.2)$$

where  $b_0$  is a constant and the subscript “S” has been added to  $\alpha$  to indicate that the discussion is now confined to the strong coupling of QCD.  $\Lambda_{QCD}$  is a parameter than can be determined experimentally; it is on the order of a few hundred MeV.<sup>10</sup> We can also express  $\alpha_S$  in the alternative form

$$\begin{aligned} \alpha_S(\mu) &= \frac{\alpha_S(\mu_R)}{1 + b_0 \alpha_S(\mu_R) \ln(\mu^2/\mu_R^2)} \\ &= \alpha_S(\mu_R) - b_0 \alpha_S^2(\mu_R) \ln(\mu^2/\mu_R^2) + \dots, \end{aligned} \quad (2.3)$$

which is more useful in evaluating the behavior of  $\alpha_S$  in the neighborhood of our chosen “subtraction point”  $\mu_R$ .

---

<sup>8</sup>The derivation of the renormalization group equation follows an equivalent line of argument.

<sup>9</sup>Actually, this characterization of  $\Lambda_{QCD}$  is misleading for two reasons. First, as  $\alpha_S$  grows close to and beyond unity, the expression for its scale dependence, obtained from some finite order calculation in perturbation theory, becomes meaningless. Second, the scale dependence of  $\alpha_S$  is impacted by threshold effects; as  $\mu$  increases into a regime where heavy quarks of a new flavor contribute significantly to loop corrections, the values of  $b_0$  and  $\Lambda_{QCD}$  change. This effective  $\Lambda_{QCD}$  is specified by replacing the generic subscript with the number of “active” flavors appropriate to a given physics process. For charm production, therefore,  $\Lambda_3$  is the most relevant incarnation of the fundamental QCD scale.

<sup>10</sup>Taking  $\Lambda_{QCD}$  to represent the mass scale of QCD, we obtain a corresponding distance scale on the order of a fermi and time scale on the order of  $10^{-21}$  seconds.

Up to this point, no physical interpretation has been given to the scale dependence of  $\alpha_S$ . After all, the scale  $\mu_R$  at which we choose to evaluate  $\alpha_S$  is arbitrary; to a given order in perturbation theory, calculated predictions of measurable quantities are insensitive to our choice. In order that perturbation theory be useful, however, a value of  $\mu_R$  must be chosen such that *both* the expansion parameter  $\alpha_S(\mu_R)$  and the logarithmic dependencies on  $\mu_R$  are small. Loosely speaking, this condition holds when  $\mu_R$  is on the order of the mass scale relevant to the physical process in question.<sup>11</sup> It is therefore common to speak of  $\alpha_S(\mu)$  as the *effective* strong coupling at the *physical* mass scale  $\mu$ .

The scale dependence of  $\alpha_S$  described above has one feature that distinguishes the strong interaction from the other forces of nature in a profound way: the effective coupling *decreases* monotonically as the mass (distance) scale increases (decreases). This behavior, known as *asymptotic freedom*, can be attributed to the presence of gluon-gluon coupling, or in other words to the fact that the vector bosons mediating the strong interaction are themselves carriers of color charge. Asymptotic freedom has the consequence that the properties of hadronic bound states cannot be treated perturbatively. On the basis of non-perturbative results,<sup>12</sup> however, it is widely believed that asymptotic freedom provides an explanation for the phenomenon of color confinement, i.e., the observation that all particles which are stable (with respect to the time scale of the strong interaction) are color-neutral. To zeroth order, this limits the possible hadronic states to baryons, mesons, and glueballs. For strong-hard-scattering processes, however, perturbative QCD calculations become more reliable as the mass scale (e.g.,  $Q^2$ ) grows.

In their calculations of charm absolute (differential) cross-sections, NDE choose  $\mu_R$  to be equal to  $m_c (2\sqrt{m_c^2 + k_T^2})$ ; a central value of 1.5 GeV is assigned to  $m_c$ . (Mangano, Nason, and Ridolfi (MNR) modify this choice in calculating differential

---

<sup>11</sup>In general, a particular process is characterized by more than one mass scale. In the case of charm production, both the charm quark mass  $m_c$  and the 4-momentum transfer  $Q^2$  define physical mass scales which are not necessarily similar in magnitude. Furthermore, if we are interested in the differential cross-section for charm quark production, the transverse momentum  $k_T$  of the charm quark also introduces a scale.

<sup>12</sup>For example, lattice QCD calculations.

cross-sections, in which case they let  $\mu_R$  equal  $\sqrt{m_c^2 + k_T^2}$ .) At this scale,  $\alpha_S$  is approximately  $\frac{1}{3}$ , too large to dismiss the possibility that higher-order terms comprise significant corrections to NLO results.

Although the NLO cross-section is independent of  $\mu_R$  to order  $\alpha_S^3$ , residual dependence of order  $\alpha_S^4$  remains.<sup>13</sup> NDE use the sensitivity of their results to factor-of-two variation of  $\mu_R$  as an ansatz estimate of the error associated with truncation of the perturbative series at NLO. The justification for this estimate is that since the full calculation to order  $\alpha_S^4$  (NNLO) must be independent of  $\mu_R$ , uncalculated NNLO terms must cancel the observed variation and are therefore similar in magnitude. But the cancellation terms thus gauged do not depend on the tree-level NNLO contributions (e.g., two gluon radiation) and indeed do not even include all of the NNLO  $\mu_R$ -dependence (e.g., that arising from two-loop renormalization of leading-order (LO) tree-level diagrams). The upper limit allowed by this uncertainty actually corresponds to adding to the NLO result a NNLO contribution estimated to be equal to the NLO contribution but enhanced through multiplication by an artificially large factor (instead of the “small”  $\alpha_S(m_c)$ ). Despite these caveats, cross-section uncertainties associated with variation of  $\mu_R$  is quantified along with other theoretical uncertainties in Sections 2.6.1 and 2.6.2.

## 2.3 Hard-scattering processes

The relevant distance scale for charm production in hadronic collisions is at most a small fraction of a fermi, indicating that the underlying processes must be described as interactions between the constituent partons of the colliding hadrons. LO diagrams are of order  $\alpha_S^2$ .<sup>14</sup> At LO, two processes contribute, namely gluon-gluon fusion and quark-antiquark annihilation; the relevant diagrams are shown in Fig. 2.1.

As mentioned previously, NDE have published full NLO calculations of total and

---

<sup>13</sup>This higher-order  $\mu_R$  dependence arises in using the renormalized  $\alpha_S(\mu_R)$  in evaluating NLO tree-level diagrams.

<sup>14</sup>Actually, the *square* of the amplitudes represented by the LO diagrams are proportional to  $\alpha_S^2$ . We will stick to the usage in the text, however, in which we equate a diagram with a physical process, which we in turn equate with that process’ effect on the charm cross-section.

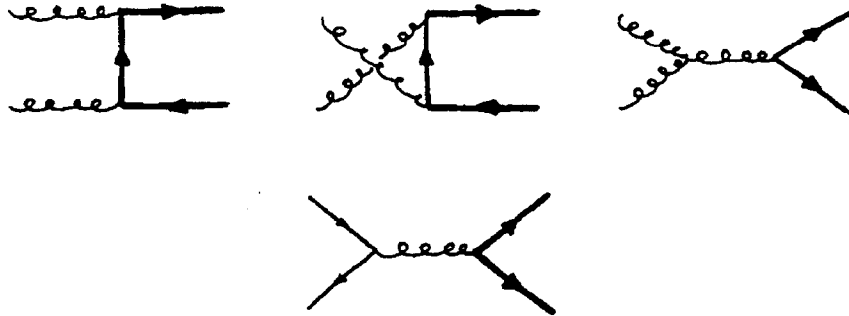


Figure 2.1: LO diagrams. Light (heavy) lines indicate light (charm) quarks.

differential cross-sections for the hadronic production of heavy quarks. At this order ( $\alpha_S^3$ ),  $gg$  fusion and  $q\bar{q}$  annihilation continue to be the most important processes; the extra vertices in these NLO diagrams are due to gluon radiation. Appearing for the first time at NLO is quark-gluon fusion, the net effect of which is only a minor (negative) adjustment to the total cross-section. Also contributing are diagrams formally of order  $\alpha_S^4$ ; interference between these “virtual” diagrams and corresponding LO processes lead to NLO terms. A sampling of some NLO diagrams is shown in Fig. 2.2. At NLO, the first loop corrections to the vertices and particle propagators appear. As discussed in the previous section, the infinities associated with these Feynman integrals are absorbed into the renormalized, scale-dependent coupling  $\alpha_S(\mu)$ . Although these loops are not explicitly shown in any of the pictured diagrams, the vertices are understood to include them.

Let a generic parton-parton interaction resulting in  $c\bar{c}$  production be represented by Fig. 2.3. The momenta of the partons from the beam and target hadrons are  $\vec{q}_B$  and  $\vec{q}_T$ , respectively. Expressions for charm production cross-sections are simplest in the partonic center-of-mass frame, in which  $q_B = q_T \equiv q$ . Treating the partons as massless, we obtain a partonic center-of-mass energy  $\sqrt{s}$  of  $2q$ . Note that in this frame,  $s$  is equal as well to the 4-momentum transfer  $Q^2$ . The threshold energy for production of a  $c\bar{c}$  pair is  $2m_c$ ; it is convenient to work with the dimensionless parameter  $\rho \equiv 4m_c^2/s$ , which has a value of 1 at threshold and decreases with increasing  $s$ . The

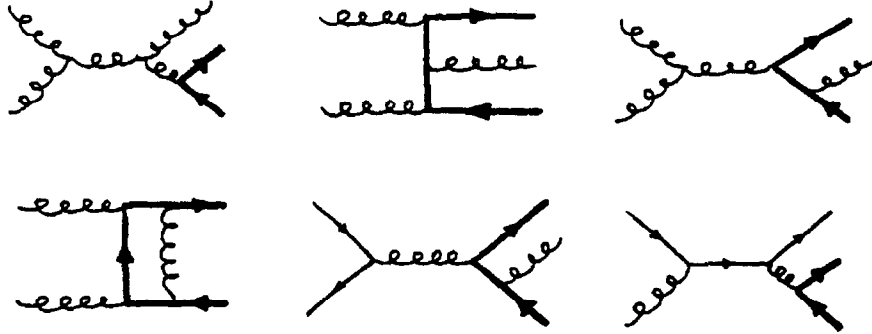


Figure 2.2: NLO diagrams. See Fig. 2.1 caption.

shaded oval in Fig. 2.3 represents the superposition of all diagrams contributing to a given order in perturbation theory. The observed charm quark (or antiquark) has a momentum  $\vec{k}$ ; the unobserved charm (and possibly a radiated gluon) account for the rest of the final state (labelled  $x$ ).

Total  $c\bar{c}$  production cross-sections (integrated over all  $\vec{k}$ ) depend only on  $\rho$  and  $m_c$ ; single-particle inclusive differential cross-sections, on the other hand, depend additionally on the magnitude of  $\vec{k}$  and its angle with respect to the axis formed by the colliding partons.

In their differential cross-section paper, NDE point out the presence of logarithmic terms which become large when  $k_T \gg m_c$ . In this limit, the heavy quark becomes effectively light, leading to final-state infrared divergences associated with gluon emission. In the kinematic range accessible to E769, however, charm quark  $k_T$  never greatly exceeds  $m_c$ .

## 2.4 Factorization

The hard-scattering amplitudes discussed in the previous section are alone not sufficient to obtain cross-section predictions for two reasons. First, in the laboratory, it is hadrons (e.g.,  $\pi$ ,  $K$ ,  $p$ ) that are accelerated into one another, not partons. Second, there is an additional class of NLO diagrams which must be accounted for in the

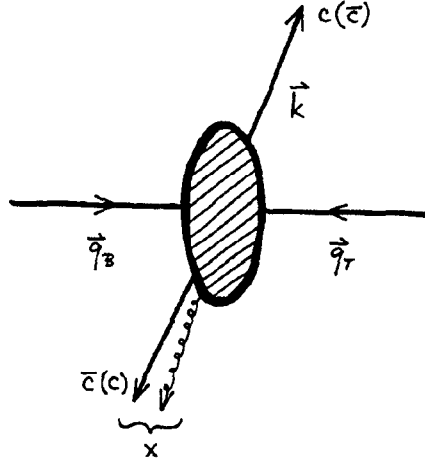


Figure 2.3: Schematic of hard-scattering kinematics.

full cross-section calculation: namely, diagrams in which one of the incoming partons radiates a gluon *before* the primary interaction occurs. These diagrams are infrared divergent, and must be regularized before a sensible result can be obtained.

Through a procedure known as factorization, both of these obstacles are removed. The hard-scattering amplitudes take as their “inputs” only the identity and momenta<sup>15</sup> of the initial state partons. Therefore, if, for each colliding hadron, the momentum distributions of each type of constituent parton are known, then the total  $c\bar{c}$  cross-section can be written as a convolution of these parton distribution functions (PDFs) with the hard-scattering cross-sections obtained by direct evaluation of the Feynman integrals.

In a procedure analogous to renormalization, infrared divergences associated with soft gluon emission are absorbed into the definition of the PDFs, rendering the aforementioned convolution products finite. As with renormalization, this subtraction of infinities must be done at some mass scale, which we label the factorization scale  $\mu_F$ . Logarithmic dependencies on  $\mu_F$  are introduced into the PDFs, leading to concomitant uncertainties in the cross-section predictions.

<sup>15</sup>Other quantum numbers are averaged over.

In this formalism, all partons within a given hadron are treated as parallel streams, the sum of whose longitudinal momenta is simply the hadron momentum  $\vec{p}_B$  or  $\vec{p}_T$ ; transverse components of the parton momenta are treated as zero.<sup>16</sup> PDFs are therefore given as functions of  $x$ , the *fraction* of the hadron’s momentum carried by the parton. More than one of each type of parton can be present in a given hadron; PDFs are therefore actually number densities, proportional at a given  $x$  value to the probability of finding a parton of momentum fraction  $x$ , where some scattering process provides the means of “finding”. Measurement of the PDFs therefore entails measuring scattering cross-sections, characterized by a certain 4-momentum transfer  $Q^2 = \mu_F^2$ , and unfolding from the aforementioned convolution the formulae relevant to the scattering involved.

The crux of the factorization theorem is that the PDFs so obtained are *independent* of the process used to measure them. This allows us to test, for example, QCD predictions for charm production using PDFs obtained by a number of various means: deep inelastic scattering of leptons (charged or neutral) on hadrons or production in hadron-hadron collisions of prompt photons or Drell-Yan pairs. In practice, PDFs obtained by simultaneous fits to data from some or all of the above processes are used [28].

This independence of PDFs on the “fate” of the extracted parton means that their  $Q^2$ -dependence is purely a QCD phenomenon, in particular a consequence of the scale dependence of  $\alpha_S$ . To illustrate this, consider the probability of extracting from a proton a  $d$  quark with momentum fraction  $x$ . In addition to the contribution of the valence  $d$ , we must account for the  $d\bar{d}$  pairs produced by constituent gluons. Any gluon with momentum fraction  $x' > x$  is a potential additional source of the desired  $d$ . Therefore, beginning at the one-loop level, the coupling strength  $\alpha_S$  directly impacts PDF evolution.

Equation 2.4 gives the single-quark charm differential cross-section; the total  $c\bar{c}$  cross-section is obtained by integrating the charm momentum  $\vec{k}$  over the full solid angle as well as the range in magnitude allowed by the kinematics.

---

<sup>16</sup>See Section 2.5 for a discussion of the consequences of relaxing this assumption.

$$\frac{d^3\sigma}{d^3k} = \sum_{i,j} \int dx_B dx_T \left[ \frac{d^3\hat{\sigma}_{ij}(x_B p_B, x_T p_{target}, \vec{k}, m_c, \mu_R, \mu_F)}{d^3k} \right] F_i^B(x_B, \mu_F) F_j^T(x_T, \mu_F) \quad (2.4)$$

In this equation,  $\hat{\sigma}_{ij}$  is the hard-scattering cross-section for partons  $i$  and  $j$  (from which infrared singularities have been subtracted) and  $F_i^{B(T)}$  is the beam (target) hadron PDF for constituent parton  $i$ . The summation runs over each two-parton combination contributing to charm production; the integrals are over the momentum fractions of each parton. The momentum of the beam (target) parton is  $x_B p_B$  ( $x_T p_{target}$ ), where  $p_B$  ( $p_{target}$ ) is the momentum of the beam (target) hadron. Note that if the partons are treated as massless, the hadronic and partonic center-of-mass energies ( $\sqrt{S}$  and  $\sqrt{s}$ , respectively) are related by

$$s = x_B x_T S. \quad (2.5)$$

The differential cross-section as written in Eq. 2.4 is not Lorentz invariant; all quantities are understood to be evaluated in the hadronic center-of-mass frame. The longitudinal momentum in this frame is converted to the dimensionless Feynman- $x$  variable ( $x_F$ ) by dividing it by  $\sqrt{S}/2$ , half the available energy, leading to the range  $-1 \leq x_F \leq 1$ .

Use of this factorized formula assumes that certain non-perturbative contributions to charm production, some of which will be discussed in the following section, are small with respect to production involving one parton from each hadron. Collins, Soper, and Sterman examined the effect of these competing processes in heavy-quark production; their conclusion was that these contributions are suppressed by powers of the ratio  $m/M$ , where  $m$  is a typical hadronic mass scale and  $M$  is the mass of the produced heavy quark [22]. Depending on how we interpret  $m$ , the charm quark mass ( $m_c \simeq 1.5$  GeV) can lead to suppression factors not particularly far from unity; it therefore remains an open question whether  $m_c$  is large enough to justify use of the factorization formalism.

## 2.5 Non-perturbative effects

As mentioned previously, a charm quark, once produced, must hadronize to *something*. As long as the time scale over which this process occurs is much longer than the strong interaction time scale characterizing the production process itself, the total  $c\bar{c}$  cross-section calculated ignoring the subsequent histories of the charm quarks should be valid, i.e., equal to one half the total charm plus anticharm particle cross-section. Interactions between a charm quark and other quarks in the event, however, will have a measurable impact on the momentum distribution of the corresponding charm hadron, leading to differences in the predicted differential cross-sections of charm quarks and, for example, charm mesons. In this section, we give only a qualitative discussion of these effects, which in general involve the exchange of soft gluons and therefore cannot be treated by perturbative methods. In addition, we mention some potential corrections to the factorized perturbative formula motivated in the previous section.

We begin with initial-state effects, some of which in principle can lead to additional mechanisms for charm production beyond those accounted for in the perturbative calculation. The first of these is flavor excitation. In this process, a  $c\bar{c}$  pair intrinsic to one of the initial-state hadrons (i.e., “sea” as opposed to valence quarks) is excited by interactions with the other hadron (via gluon exchange), giving the virtual heavy quark pair enough energy to reach its mass shell. The results of an early theoretical study by Cambridge suggested that the charm cross-section attributable to flavor excitation alone was potentially greater than that from LO “flavor creation” processes [23]. Subsequent investigations showed, however, that this process, whose diagram is topologically equivalent to standard  $gg$  fusion graphs, is thereby included at some level in the perturbative result [22]. NDE therefore calculate  $c\bar{c}$  cross-sections using PDFs with no explicit charm sea component, including flavor excitation as a higher-order correction (i.e., as a component of  $gg$  fusion). More recently, Tung and collaborators have developed a method of fully incorporating both flavor creation and excitation by explicitly subtracting from the sum of the two processes the region of kinematic overlap. The net addition due to flavor excitation is found to grow large only for

production well above threshold (i.e.,  $k_T \gg m_c$ );<sup>17</sup> we therefore do not expect the E769 results to be sensitive to this effect.

Related to the flavor excitation process is the concept of intrinsic charm, introduced by Brodsky and collaborators [21]. In this picture, hadronic wavefunctions contain Fock state components in which a  $c\bar{c}$  pair carries most of the hadronic momenta. For example, a proton  $|uud\rangle$  would contain a  $|uudc\bar{c}\rangle$  component. Note that these charm components are *not* equivalent to the virtual charm sea generated by QCD evolution of the PDFs. Originally motivated by CERN-ISR measurements of anomalously high charm particle cross-sections at high  $x_F$ ,<sup>18</sup> the intrinsic charm component of the proton was estimated to be on the order of 1-2%. Recent (null) measurements of diffractive charm production in 800 GeV  $p$ -Si interactions, however, have been interpreted as imposing an upper limit of 0.2% on the intrinsic charm component of the proton [31].

The longitudinal ( $x_F$ ) and transverse ( $p_T$ ) momentum distributions of charm particles should in principle differ from those predicted for charm quarks, due to the interaction of the latter with other quarks in the event, both spectator valence quarks and light  $q\bar{q}$  pairs created from the vacuum. The process by which charm quarks coalesce with light quarks to form color-neutral bound states is known as hadronization or fragmentation. Even before this stage is reached, however, the factorized formula developed above may neglect an important input to predicting the charm *quark* distributions, namely the intrinsic  $p_T$  of constituent partons. On the basis of the transverse spatial confinement of the partons, we might expect transverse momenta on the order of  $\Lambda_{QCD}$  – a few hundred MeV. MNR, in a study based on a HERWIG Monte Carlo simulation, find that a LO calculation assuming an average intrinsic  $p_T$  of 1.5-1.7 GeV is sufficient to reproduce MC results for charm quark distributions (which they admit should not be taken as a universal benchmark) [32]. The effect of this intrinsic  $p_T$  is a “uniform smearing” of the transverse distributions; for a cross-section exponentially

---

<sup>17</sup>Actually, this method was first developed to describe heavy quark *lepto*production [5]. An analogous treatment of hadroproduction is in progress; preliminary results were presented at DPF96 [39].

<sup>18</sup>For an extensive review of early charm hadroproduction measurements, see the two review articles given in [42].

falling with  $p_T$ , the net effect of such smearing is a hardening of the distribution.

In treating the effect of hadronization on charm distributions, the assumption of universal fragmentation is sometimes made. In this picture, the ratio of the charm hadron momentum to that of its “parent” charm quark is given by a probability distribution (the fragmentation function) which is independent of the process by which the charm quark is produced, for example through  $e^+e^-$  collisions. The charm quark is essentially seen as the progenitor of an isolated jet; its momentum is degraded by the energy lost in the creation of light  $q\bar{q}$  pairs. In hadronic collisions, however, the environment is sufficiently different to call this procedure into question.<sup>19</sup> For example, coupling between low- $k_T$  charm quarks and co-moving spectator quarks can lead to charm hadrons whose momenta are enhanced with respect to that of their charm parents; this effect is known as “color-dragging” and is related to another consequence of charm-spectator coalescence, namely the “leading-particle” effect.

A leading charm particle is defined, for  $x_F > 0$ , as one which shares at least one light valence quark or antiquark flavor with the beam particle. An example of a leading particle in  $\pi^-$ -induced production is  $D^-$ . At high  $x_F$  especially, we expect the proximity of the charm quark to the forward spray of beam fragments to lead to an enhanced cross-section for charm species which result from hadronization with these co-moving spectators. This effect has been measured to be significant and to increase at high  $x_F$ .<sup>20</sup> In this thesis we will make a distinction between non-leading and neutral-leading particles. A non-leading particle is defined as the charge conjugate of a leading particle (e.g.,  $\pi^-$ -induced  $D^+$  mesons).<sup>21</sup> A neutral-leading particle, on the other hand, is defined as any particle for which both particle *and* antiparticle are *not* leading (e.g.,  $K^+$ -induced  $D^0$  mesons). For species which are otherwise similar, a leading particle will be more likely to have undergone color-dragging than non-leading or neutral-leading particles; therefore, we expect leading particles to exhibit harder

---

<sup>19</sup>MNR have also pointed out that application of fragmentation functions to longitudinal distributions is not boost-invariant and can lead to significantly different results in different frames [32].

<sup>20</sup>See Section 8.3.4 and references quoted therein.

<sup>21</sup>In the case of a *neutral* beam particle, this definition must be modified, as both particle and antiparticle can be leading (e.g.,  $\pi^0$ -induced  $D^+$  and  $D^-$  mesons). We state this only for completeness, as E769 uses only charged beams.

$x_F$  distributions.

## 2.6 Predictions and uncertainties

MNR have made available the program HVQMNR, which they used to generate the NLO QCD heavy-quark cross-section predictions (absolute and differential) presented in [32].<sup>22</sup> This program allows for variation of beam energy ( $E_B$ ), the identities of the initial-state hadrons (constrained by the availability of the appropriate PDFs),  $\Lambda_{QCD}$ ,  $\mu_R$ ,  $\mu_F$ , and the mass of the produced heavy quark. In this section we employ this program, using the default parameters listed below (those of MNR), to obtain predictions with which to compare our measured forward and differential cross-sections.<sup>23</sup>

$$E_B = 250 \text{ GeV}$$

$$\text{beam particle (PDF)} = \pi^- \text{ (SMRS2), } p \text{ (HMRSB)}$$

$$\text{target particle (PDF)} = N \text{ (HMRSB)}$$

$$\mu_R = \mu_0$$

$$\mu_F = 2\mu_0$$

$$\mu_0 = \begin{cases} m_c & \text{absolute} \\ \sqrt{m_c^2 + k_T^2} & \text{differential} \end{cases}$$

$$m_c = 1.5 \text{ GeV}$$

$$\Lambda_5^a = 122 \text{ MeV}$$

---

<sup>a</sup> $\Lambda_5$  is connected to the more relevant  $\Lambda_3$  through the NDE renormalization scheme.

PDFs are available for the pion and proton, but not for the kaon; predictions are therefore made only for charm production induced by  $\pi^-$  and  $p$ .<sup>24</sup> MNR use SMRS2 (HMRSB) parametrizations of  $\pi^-$  ( $p$ ) PDFs; these PDF sets are defined and discussed in [28] and are plotted in Fig. 2.4 at  $Q^2 = 4 \text{ GeV}^2$ .

---

<sup>22</sup>The NLO QCD results published by MNR differ from those of NDE due to the former's use of more modern PDFs.

<sup>23</sup>We verified our correct use of HVQMNR by reproducing numerical results for absolute and differential cross-sections presented by MNR in [32] and in their follow-up paper [26], for which they were joined by Frixione (FMNR).

<sup>24</sup>Although  $\pi^+$  PDFs should be completely determined by those for  $\pi^-$ , HVQMNR as written does not differentiate between the two; therefore, only predictions for  $\pi^-$ -induced production are

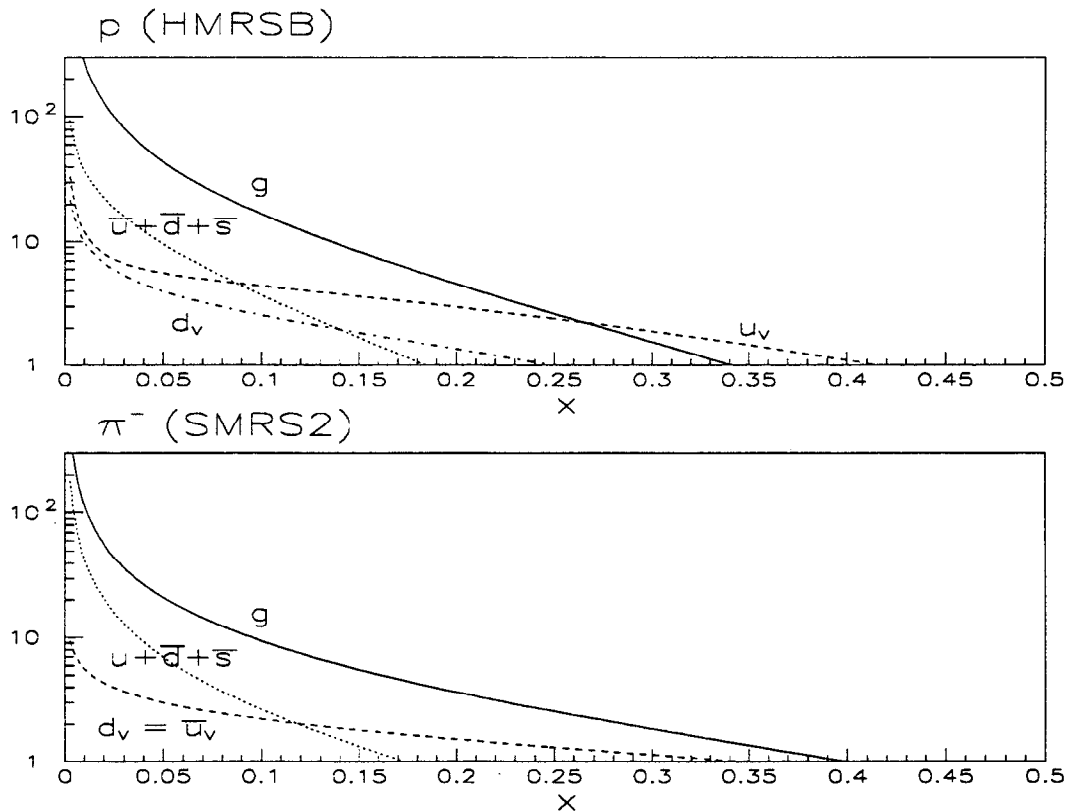


Figure 2.4: Parton distribution functions at  $Q^2 = 4 \text{ GeV}^2$ .

Precise comparison of the contributions different processes make to charm production is not possible until the hard-scattering cross-sections are convolved with the appropriate PDFs. Assuming for the moment that amplitudes for all processes are equal and independent of  $\rho$  (in the production region  $\rho < 1$ ), we can estimate the relative importance of  $gg$  fusion and  $q\bar{q}$  annihilation by direct inspection of Fig. 2.4. For E769,  $\sqrt{S} = 21.7 \text{ GeV}$ , leading to the relation

$$x_B x_T \geq \frac{4m_c^2}{S} = \left( \frac{2 \times 1.5 \text{ GeV}}{21.7 \text{ GeV}} \right)^2 = 0.019 < \rho. \quad (2.6)$$

A general feature of PDFs is that they fall very rapidly with rising  $x$ ; therefore,  


---

 available.

given our aforementioned assumption, charm production should be dominated by those regions in the  $x_B$ - $x_T$  plane close to the hyperbola defined by  $x_B x_T = 0.019$ . If we further assume that in this neighborhood the PDFs are falling exponentially, we find that most production occurs at the point on the hyperbola where  $x_B = x_T = \sqrt{0.019} = 0.14$ . Comparing  $g(x)$  and  $\bar{q}(x)$  distributions at  $x_B = 0.14$ , we expect  $gg$  fusion to dominate over  $q\bar{q}$  annihilation, especially in  $pN$  collisions, where the only source of antiquarks is the sea.

This conclusion is borne out by the complete HVQMNR calculation, which indicates that  $gg$  fusion constitutes 80% (89%) of charm production in  $\pi^- N$  ( $pN$ ) collisions at E769's center-of-mass frame energy.<sup>25</sup> The balance of the cross-section is attributable to  $q\bar{q}$  annihilation,  $qg$  processes providing at NLO only an insignificant correction. The *shapes* predicted for charm quark differential distributions are not affected greatly by the inclusion of NLO terms in the perturbative calculation [32]. In an absolute sense, however, the NLO contribution is very important, approximately *doubling* the  $c\bar{c}$  cross-section prediction.

In Sections 2.6.1 and 2.6.2, we present NLO QCD predictions for absolute  $c\bar{c}$  and differential  $c$  quark production cross-sections, respectively; these predictions are given for  $\pi^- N$  and  $pN$  interactions. In addition, the uncertainties in these results will be discussed and estimated, based on MNR and FMNR results. Direct comparisons of these predictions with E769 and previous measurements will be made in Sections 8.3.1 and 9.3.1.

## 2.6.1 Absolute cross-sections

The predicted  $c\bar{c}$  cross-sections for 250 GeV  $\pi^-$  and  $p$  collisions on a nucleonic target are similar: 5.2 and 4.5  $\mu\text{b}/\text{nucleon}$ , respectively.<sup>26</sup> For  $pN$  production, we could

---

<sup>25</sup>In the remainder of this chapter, statements concerning NLO QCD predictions for charm production should be understood as applying at E769's energy, i.e.,  $\sqrt{S} = 21.7$  GeV.

<sup>26</sup>The dominant  $gg$  fusion component of the cross-section depends rather simply on the distribution of gluons in the beam particle:

$$\sigma_{gg} \propto \langle xg \rangle_{thr} - x_{thr} \langle g \rangle_{thr},$$

where  $\langle g \rangle_{thr}$  and  $\langle xg \rangle_{thr}$  are the first two moments of the gluon distribution above an effective charm threshold  $x_{thr} \sim 0.04$ . The cross-section essentially increases linearly with the fraction of

compare this number directly to the measured total charm plus anticharm *particle* cross-section in the forward hemisphere, if this latter result were available.<sup>27</sup> In the case of  $\pi^-$ -induced production, however, the relative hardness of the gluons in the pion leads to asymmetric production in the hadronic center-of-mass frame, resulting in more charm particles with  $x_F > 0$ . MNR have determined the ratio  $\frac{\sigma_{c\bar{c}}(x_F > 0)}{\sigma_{c\bar{c}}}$  to be about 5/8 over a wide range in  $E_B$ , where  $\sigma_{c\bar{c}}(x_F > 0)$  is defined as the  $c\bar{c}$  pair production cross-section with a cut of  $x_F > 0$  placed on the charm quark. In this case, therefore, we must multiply the QCD prediction by a factor  $\frac{5}{8} \times 2 = 1.25$  before an analogous comparison can be made.<sup>28</sup>

As detailed in the previous sections, potentially significant theoretical uncertainties in  $\sigma_{c\bar{c}}$  are associated with each of the important input parameters of the calculation:  $m_c$ ,  $\mu_R$ ,  $\mu_F$ ,  $\Lambda_{QCD}$  (through which we obtain the uncertainty in  $\alpha_S$ ), and the PDFs. We report here on those which are likely to be most significant.

MNR find that decreasing  $m_c$  by 100 MeV leads to a 50% increase in the prediction for  $\sigma_{c\bar{c}}$ . If we assume an uncertainty of  $\pm 300$  MeV in  $m_c$  about the central value of 1.5 GeV, we find that the resulting error band in the prediction spans a full order of magnitude! Decreasing  $\mu_R$  also leads to an increased cross-section prediction; multiplying (dividing) the default value of  $\mu_R$  (in this case,  $m_c$ ) by a factor of two decreases (increases)  $\sigma_{c\bar{c}}$  to about 40% (200%) of its central value. Due to difficulties associated with varying  $\mu_F$  below scales for which PDF parametrizations are available, MNR do not attempt to quantify the analogous uncertainty associated with this scale; they do note, however, that it could be as large as that for  $\mu_R$ . Clearly, the errors already cited show that the precision of current theoretical predictions for  $\sigma_{c\bar{c}}$  (even assuming the validity of factorized perturbative QCD formulae at NLO) lag far behind that achieved experimentally (on the order of 10-20%, in some cases).

---

momentum carried by the gluons above this threshold, adjusted by a small negative correction which increases with the number of gluons among which this momentum must be divided.

<sup>27</sup>In practice, we obtain cross-section measurements only for a portion (albeit the expected bulk) of the charm hadrons; in Section 8.3.1, the issues surrounding this comparison of data and theory are discussed.

<sup>28</sup>This factor would be slightly more complicated if the signs of  $x_F$  for the produced  $c$  and  $\bar{c}$  quarks exhibited dependence on one another; MNR find that they are approximately uncorrelated.

## 2.6.2 Differential cross-sections

In this section, we present NLO QCD differential cross-section predictions for charm *quarks*. The HVQMNR program is used to obtain shape predictions and to study their sensitivity to variations of theoretical parameters over ranges deemed reasonable by MNR. No attempt is made to model or calculate the various non-perturbative effects described in Section 2.5; as stated previously, however, their impact on charm *particle* distributions is potentially significant. With this said, we drop the notational distinction between charm quark  $k_T$  and charm particle  $p_T$ ; the symbol “ $p_T$ ” is hereafter used to represent transverse momentum in both cases.

The predicted  $d\sigma/dx_F$  and  $d\sigma/dp_T^2$  shapes, for both  $\pi^-N$  and  $pN$  interactions, are plotted in Figs. 2.5 and 2.6. Empirical fits to these distributions, described below, are also shown.

The  $d\sigma/dx_F$  shapes are well-fit by the following function in the experimentally-accessible range  $-0.1 < x_F < 0.8$ :

$$d\sigma/dx_F = \begin{cases} N' \exp -\frac{1}{2}\left(\frac{x_F-x_c}{\sigma}\right)^2, & |x_F - x_c| < x_b \\ N(1 - |x_F - x_c|)^n, & |x_F - x_c| > x_b. \end{cases} \quad (2.7)$$

At the boundaries between the central and tail regions ( $x_c \pm x_b$ ), the function and its derivative are forced to be continuous through the following constraints:

$$\sigma = \sqrt{\frac{x_b(1 - x_b)}{n}} \quad (2.8)$$

$$\ln \frac{N'}{N} = n \left( \frac{x_b}{2(1 - x_b)} + \ln(1 - x_b) \right). \quad (2.9)$$

Thus the shape of  $d\sigma/dx_F$  can be described over this range with three free parameters:  $x_c$ ,  $x_b$ , and  $n$ . As detailed in Section 9.3.1, our measured  $x_F$  distribution shapes, given the precision with which they are determined, require only a 1-parameter function (Equation 9.9) be used for fitting. In comparing theory and data, therefore, we will follow the procedure of fitting data distributions to theoretical shapes directly rather than comparing parameters. For the sake of completeness, the theoretical fit parameters are given in Table 2.1. As expected from the relative average hardness of

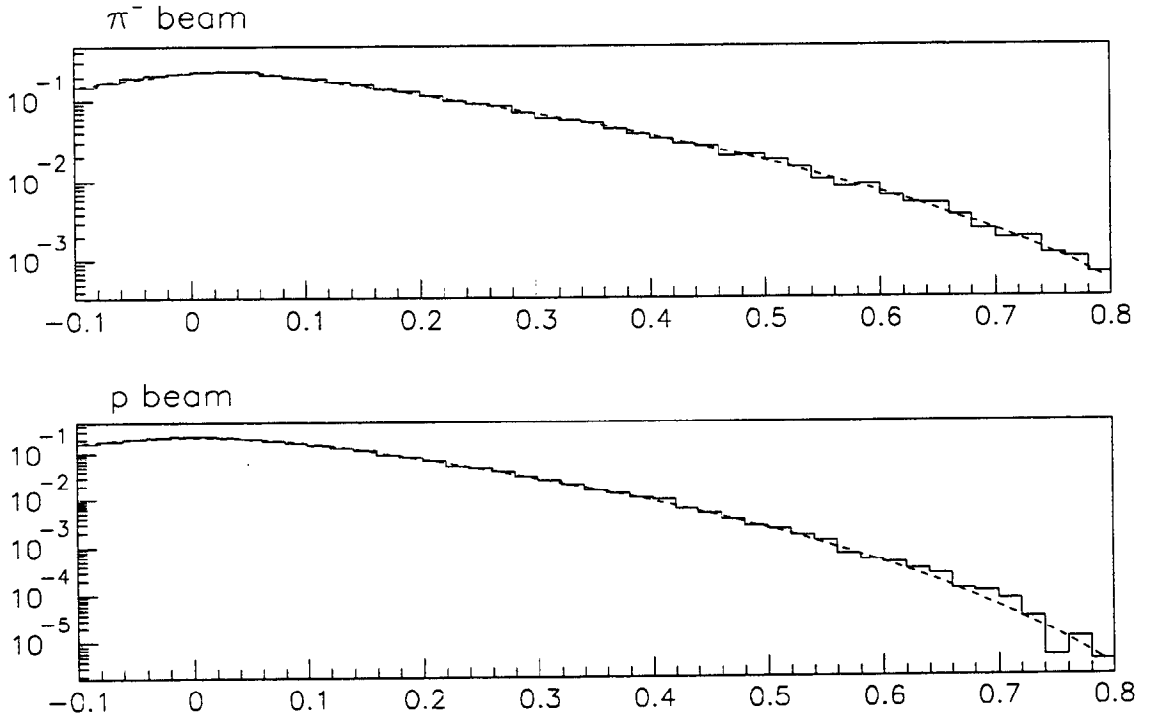


Figure 2.5: QCD NLO  $c$  quark  $d\sigma/dx_F$  vs.  $x_F$ . The distributions are integrated over the full  $p_T$  range. Normalization is arbitrary.

the gluons in pions with respect to those in protons,<sup>29</sup> the predicted  $d\sigma/dx_F$  distribution in  $\pi^- N$  production falls less rapidly with  $x_F$  (i.e., has a lower  $n$  value) and is centered in the forward hemisphere (i.e.,  $x_c > 0$ ).

The theoretical predictions for  $d\sigma/dp_T^2$  are well-parametrized over the entire  $p_T^2$  range by the following function, introduced by FMNR:

$$d\sigma/dp_T^2 = N (\alpha m_c^2 + p_T^2)^{-\beta}, \quad (2.10)$$

where  $m_c$  is the mass of the charm quark. Results of these fits (with  $m_c$  set to 1.5

<sup>29</sup>On average, gluons carry a larger fraction of momentum in the proton (47%) than in the pion ( $\sim 38\%$ ). But since the average number of gluons in the proton (19) is more than twice that in the pion (9), the average momentum *per gluon* is significantly higher in the pion.

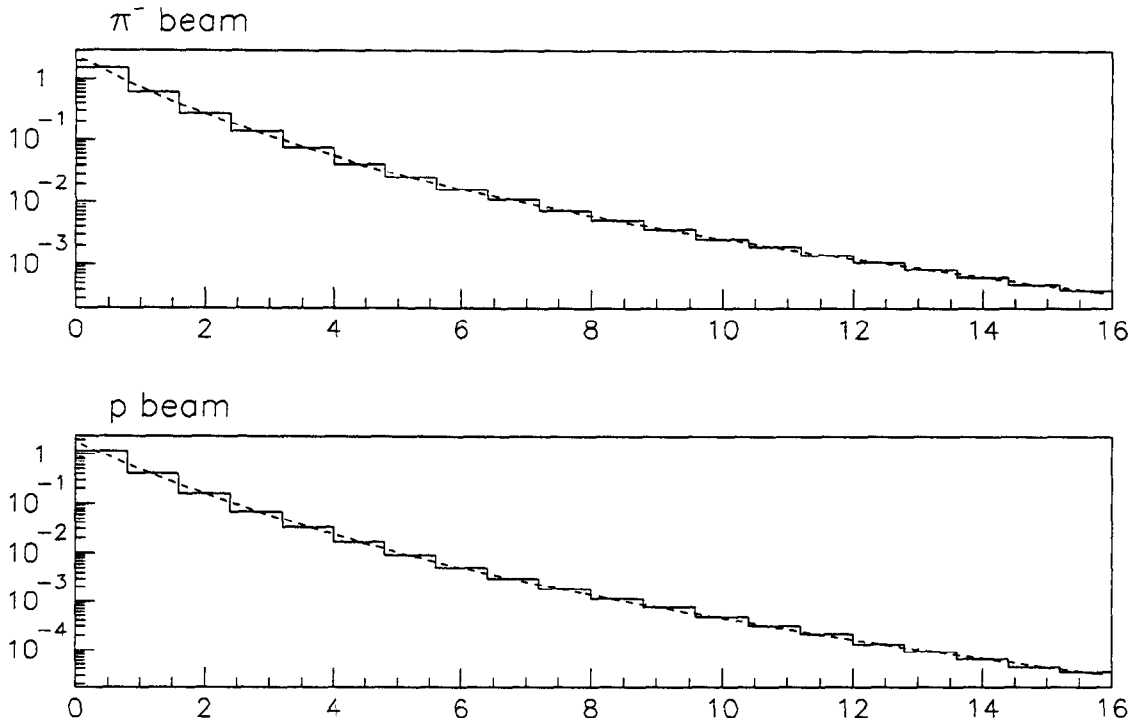


Figure 2.6: QCD NLO  $c$  quark  $d\sigma/dp_T^2$  ( $\text{GeV}^{-2}$ ) vs.  $p_T^2$  ( $\text{GeV}^2$ ). The distributions are integrated over the forward hemisphere ( $x_F > 0$ ). Normalization is arbitrary.

GeV) are given in Table 2.2. Although the predicted fall-off in  $p_T^2$  is more rapid in  $p$ -induced production, the beam-particle dependence here is less pronounced than in the  $x_F$  distributions (and therefore more easily compromised by non-perturbative effects).

In Figs. 2.7 and 2.8, changes in the predicted  $\pi$ -induced distributions due to variation of some of the theoretical input parameters are shown;  $p$ -induced distributions are also given as a reference by which to judge these theoretical uncertainties. The different  $\pi^-$  PDFs referred to in the caption of Fig. 2.8 correspond to varying the fraction of pion momentum carried by gluons by  $\pm 5\%$  from the default amount used in SMRS2.

In general, the sensitivity of the shapes to these variations is small compared to

Beam	$x_c$	$x_b$	$n$
$\pi^-$	0.028	0.040	4.19
$p$	0.000	0.145	7.39

Table 2.1:  $d\sigma/dx_F$  theory shape parameters.

Beam	$\alpha$	$\beta$
$\pi^-$	1.76	5.45
$p$	2.66	8.46

Table 2.2:  $d\sigma/dp_T^2$  theory shape parameters.

the difference in the shapes expected in  $\pi N$  and  $pN$  production. The only exception is the effect of variation of  $m_c$  (by  $\pm 300$  MeV) on the  $d\sigma/dp_T^2$  distributions; the  $\pi$  and  $p$  beam predictions tend to change similarly with these variations, however, leaving the difference in their shape parameters fairly stable. On the right-hand side of Fig. 2.8, the effects of  $m_c$  variations on  $\pi$  and  $p$ -induced  $p_T^2$  distribution shapes are shown simultaneously.

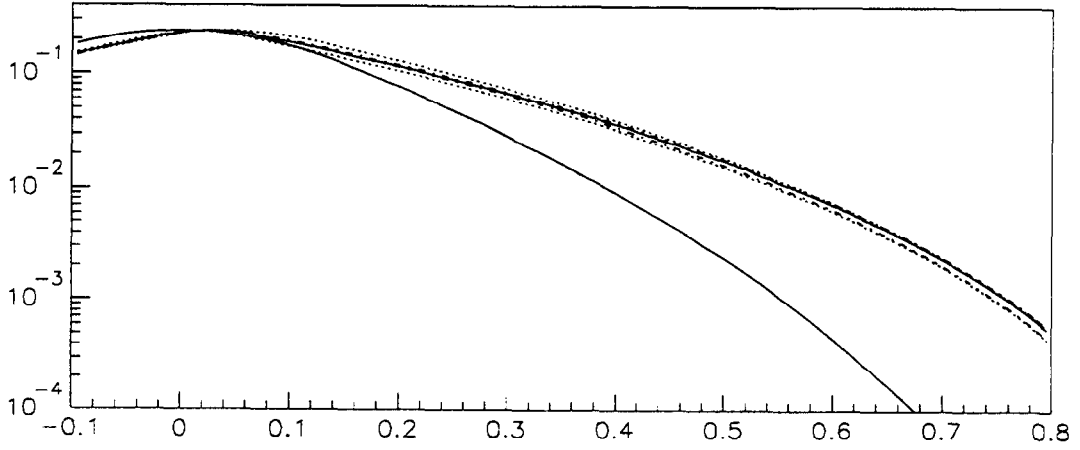


Figure 2.7: QCD NLO  $c$  quark  $d\sigma/dx_F$  vs.  $x_F$ , default (solid, upper =  $\pi$ , lower =  $p$ ), variation of  $\mu_R$  by factor of 2 (dashed), variation of  $m_c$  by 300 MeV (dotted). Normalization is arbitrary.

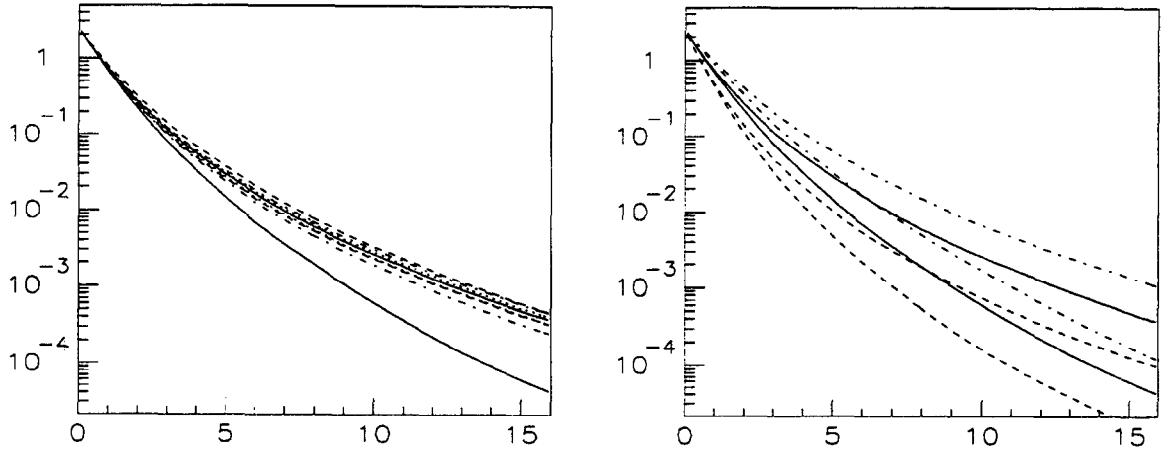


Figure 2.8: QCD NLO  $c$  quark  $d\sigma/dp_T^2$  ( $\text{GeV}^{-2}$ ) vs.  $p_T^2$  ( $\text{GeV}^2$ ); default (solid, upper =  $\pi$ , lower =  $p$ ); Left: variation of  $\mu_R$  (dashed) and  $\mu_F$  (dash-dotted) by factor of 2, different  $\pi^-$  PDF sets (dotted); Right:  $m_c = 1.2$  GeV (dash-dotted),  $m_c = 1.8$  GeV (dashed). Normalization is arbitrary.